The mechanism and suppression of physisorbed-water caused hysteresis in graphene FET sensors

Miroslav Bartošík*(1,2,3), Jindřich Mach(1,2), Jakub Piastek(1,2), David Nezval(2), Martin Konečný(2), Vojtěch Švarc(1,2), Klaus Ensslin(4) and Tomáš Šikola(1,2)

(1) Central European Institute of Technology – Brno University of Technology (CEITEC BUT) Purkyňova 123, 612 00 Brno, Czech Republic

(2) Institute of Physical Engineering, Brno University of Technology, Technická 2, 616 69 Brno, Czech Republic

(3) Department of Physics and Materials Engineering, Faculty of Technology, Tomas Bata University in Zlín, Vavrečkova 275, 760 01 Zlín, Czech Republic

(4) *Solid State Physics Laboratory, ETH Zürich, CH 8093 Zürich, Switzerland*

*bartosik@fme.vutbr.cz

Abstract:

Hysteresis is a problem of field-effect transistors (FET) often caused by defects and charge traps inside a gate-isolating (e. g. SiO_2) layer. This work shows that graphene-based FETs also exhibit hysteresis due to water physisorbed on top of graphene determined by a relative humidity level which naturally happens in biosensors and ambient operating sensors. The hysteresis effect is explained by trapping of electrons by the physisorbed water and it is shown that this hysteresis can be suppressed using short pulses of alternating gate-voltage.

Keywords: Graphene, Sensor, Relative humidity, Water, Hysteresis, Gate-voltage, Physisorption

Graphene, a single layer of carbon atoms arranged into hexagonal structure, is a suitable material for electronic sensors working on a principle of resistivity changes caused by adsorbed molecules acting as acceptors or donors. It has been shown that in vacuum a graphene-based sensor can detect even single gas molecules[1]. This extremely high sensitivity results from the fact that every graphene atom is a surface atom itself and can directly interact with adsorbed particles. Moreover, due to graphene's biocompatibility and ability to be easily functionalized, it can be advantageously used in biosensors operating in air or even in a water solution. Here, in addition to detected molecules, graphene is exposed to water molecules influencing real sensor behavior[2].

The specific species are usually sensed by graphene sensors (biosensors) having a field-effect-transistor (FET) arrangement. The main characteristic for detection of these species is the dependence of resistivity on back-gate voltage (back-gate trace) exhibiting a peak corresponding to the charge neutrality point (CNP peak). This point is defined by the Fermi level crossing the Dirac point, where total charge in graphene should be zero. Ideally, in case of sensors the shift of the CNP peak is determined by doping caused by adsorbed molecules being detected. However, the real graphene sensors of a FET's design generally exhibit a hysteresis in atmospheric and water-solution conditions consisting in different

positions of the CNP peak during upward and downward back-gate voltage sweeping. Such a behavior is often attributed to charge trapping and diffusion inside a gate-isolating layer (e. g. ion diffusion, negative/positive bias temperature instability)[3–13,14]. This behavior causes ambiguity in determination of graphene doping level, and corresponding amount of detected molecules.

In this work we show that hysteresis in a graphene FET sensor is caused also by physisorptively adhered water molecules. The water origin of this hysteresis is proved by measurements at different relative humidity: under atmospheric conditions and in a vacuum environment caused by water molecules only. Furthermore, it is shown that the hysteresis can be suppressed by utilization of alternating short gate-voltage pulses. Finally, a fundamental mechanism of electron trapping by physisorbed water explaining the hysteresis behavior is proposed.

METHODS

A large area polycrystalline graphene layer was grown by a standard low-pressure CVD method[15]. To get a high quality graphene layer, an ultrasmooth copper foil was used for graphene growth[16,17,18]. The growing procedure consisted of three technology steps: (1) copper annealing at a hydrogen flow (4 sccm, 10 Pa, 1000 °C, 30 minutes) to remove air adsorbates, (2) methane introduction (40 sccm, 70 Pa, 1000 °C, 30 minutes) to grow graphene in a H_2/CH_4 mixture, and (3) bottom-side-copper cleaning in an oxygen-argon plasma (20% O2, 80% Ar, 2 minutes) to remove graphene from this side, while that one from the top side was protected from plasma etching by a spin-coated PMMA layer.

The transfer process was performed by a PMMA-assisted wet transfer method. Graphene was transferred on a p-doped silicon substrate (resistivity 1.0×10^{-3} - 1.5×10^{-3} Ω·cm) covered by thermal 280 nm SiO2 and two lithographically prefabricated Au(45 nm)/ Ti (3 nm) electrodes. The active part of graphene between these electrodes then determines a geometry of the measured graphene channel with the length L = 50 μm and width W = 400 μm.

The sample is arranged in the form of a field effect transistor (FET) with a bottom gate-electrode to provide back-gate voltage sweeping (Fig. 1 a). The application of back-gate voltage (V_G) controls a charge

carrier density according to the formula $n = (\varepsilon_0 \varepsilon_r / ed) V_G$, where ε_0 is the vacuum permittivity, ε_r is the SiO_2 relative permittivity(3.9), e is the elementary charge and d is the thickness of the SiO_2 layer. The graphene resistivity is then defined as $\rho = RW/L$ and its dependence on V_G determines the doping type and charge carrier mobility. The resistance *R* of the graphene layer was measured using a lock-in amplifier SR830 (Stanford Research Systems) with a frequency of 1333 Hz, fixed current of 100 nA, and back-gate voltage in a range of ±90 V.

All transport experiments were measured in-situ at controlled relative humidity (RH) and room temperature of 25 °C (RT). The experiments were carried out either in a home-built stain-less steel environmental chamber (Fig. 2 b) under ambient conditions at atmospheric pressure (10^5 Pa) or in another home-built ultra-high vacuum (UHV) chamber providing low base-pressure (4×10^{-7} Pa) that was increased only by introducing water vapors up to 3000 Pa (corresponding to 95% RH). Nitrogen gas or a water vapor – nitrogen mixture can be flowed through the environmental chamber to reduce or increase RH in the chamber, respectively[19]. In the UHV chamber the total pressure is controlled by evaporation of water from a flask into vacuum.

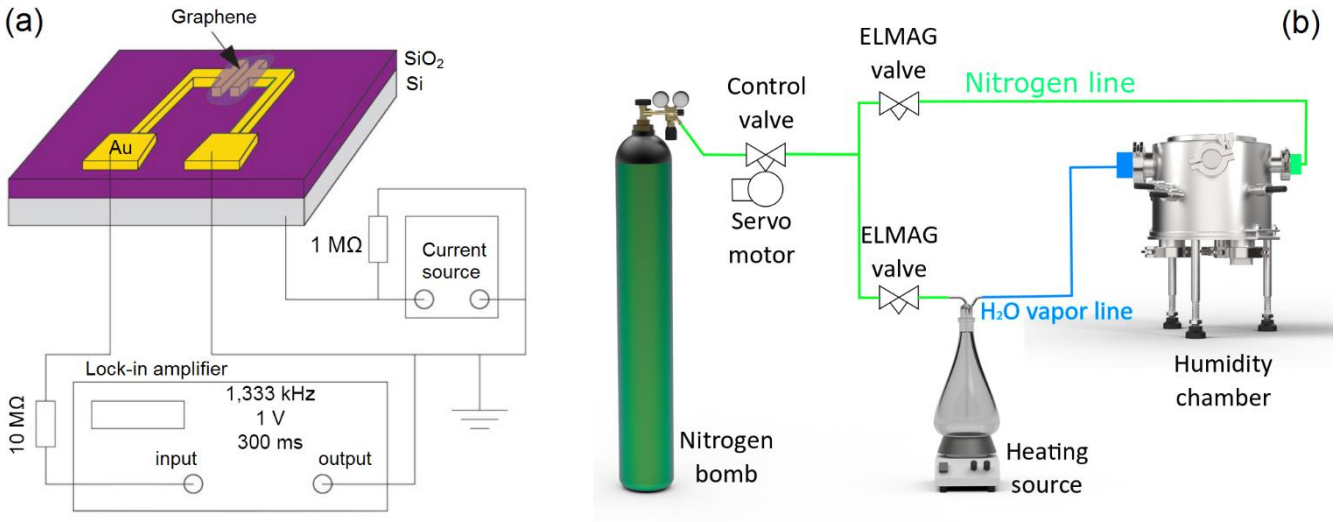

FIG. 1. (a) Schematic of a sensor electronic setup for transport measurements. (b) Environmental chamber for controlling the relative humidity.

EXPERIMENTAL RESULTS

Back-gate trace in vacuum and atmosphere at different RH

A typical back-gate trace experiment in atmospheric conditions is depicted in Fig. 2 (a). Here, the gate voltage was continuously swept from 0 V to 90 V, from 90 V to -90 V, and finally from -90 V to 0 V. The voltage incremental change during one step was 1 V and its duration 0.6 Vs^{-1}. The measurement was performed at three values of relative humidity: 10%, 40%, and 70%. Obviously, there are two distinct ways of behavior. First, the curves are moved towards positive voltages with relative humidity that corresponds to a stronger p-doping of graphene. Second, the individual curves for each RH do not overlap, and exhibit a strong hysteresis. For lower RH of 10% and 40%, the hysteresis can be quantified by a voltage-shift (ΔV_G) of the CNP peak, which was 15 V and 19 V, respectively. For higher RH of 70% the voltage-shift parameter cannot be determined due to a strong p-doping moving the CNP peak out of the measured range. However, even here a strong hysteresis is present. Generally, the hysteresis causes that the CNP peak is moved to higher gate-voltages for increasing gate voltage, and to lower gate-voltages for decreasing gate voltage during one cycle of back-gate trace.

The hysteresis in measurement leads to an ambiguity in determination of the CNP peak position, and consequently influences the calculation of the charge carrier concentration. This ambiguity is possible to quantify. For example, in case of a back-gate trace for 10% RH (red curve in Fig. 2 a), the right CNP peak occurs at gate-voltage of 74 V, and the left peak at 59 V that corresponds to the mentioned 15 V voltage-shift. It results in a charge carrier concentration 5.7×10^{12} cm^{-2} for the right CNP peak position and 4.54×10^{12} cm^{-2} for the left CNP peak. Therefore, the absolute ambiguity (error) in determination of charge carrier concentration is 1.16×10^{12} cm^{-2} and the corresponding relative error in finding this concentration with respect to the mean value is almost 23% (1.16 / (5.70 + 4.54) / 2). This is a quite high value as the changes in the CNP peak position caused by a detected substance in a typical sensor or biosensor are often much smaller[20–26].

The hysteresis disappeared when the sample was put into the UHV chamber and the pressure was pumped down to 10^{-7} Pa as can be seen in Fig. 2 (b), (blue curve). Furthermore, after annealing at a temperature of 300 °C for 1 hour the CNP peak was shifted from 72 V to 1 V (red curve), and the sample again revealed no hysteresis. It leads to the following conclusions. First, the removal of atmospheric molecules in space surrounding the sample eliminated the hysteresis. Second, the annealing, which generally removes surface contaminants, adsorbed water molecules and even water confined under graphene (at the silica-graphene interface)[27], changed the strongly p-doped graphene to intrinsic graphene.

In order to distinguish between the influence of water and other atmospheric molecules (oxygen, nitrogen, etc.), the annealed sample was exposed in the UHV vacuum chamber to water molecules only as shown in Fig. 2 (c). Introducing water vapor into the chamber up to the pressure 3000 Pa (partial pressure of water molecules is here also an absolute pressure) resulted in restoring of hysteresis behavior. The voltage-shift parameters (ΔV_G) characterizing the hysteresis rate were 14 V, 24 V, and 27 V for water vapor pressures 224 Pa, 1150 Pa, and 3000 Pa, respectively. It corresponds to a relative humidity of 7%, 36%, and 95%. It means that the hysteresis was increasing with the amount of water vapor. A more detailed measurement in the relative humidity range from 0% to 36% RH (Fig. 2 d) showed a gradual exponential saturation of hysteresis development with water vapor pressure ($\approx 23.72 - 20.22 \cdot e^{-0.003 \cdot p}$).

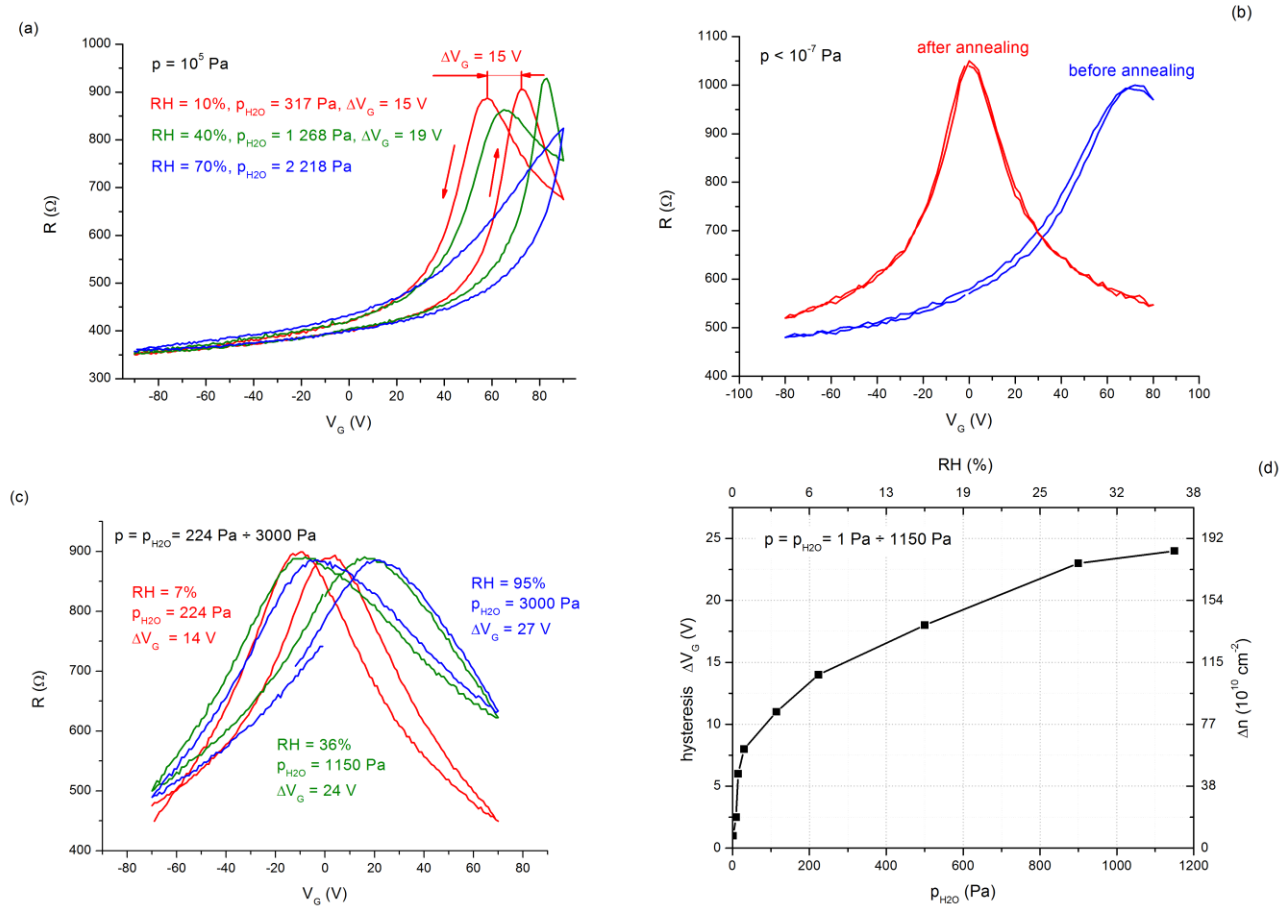

Fig. 2. Evolution of hysteresis during measurement of graphene resistance as a function of back-gate voltage: (a) in atmospheric conditions at three different RH, (b) in UHV before and after annealing (no hysteresis), and (c) in low vacuum at three different water vapor pressures (after introducing water vapors into an UHV chamber). (d) Hysteresis as a function of pressure of water vapor introduced into a vacuum chamber.

Comparing hysteresis using the back-gate voltage-shift (ΔV_G) for experiments performed in atmospheric (Fig. 2 a) and vacuum conditions (Fig 2 c), it is obvious that the hysteresis has very similar values for comparable RHs. On the other hand, the average p-doping shift of CNP (calculated from the corresponding left and right peaks in Fig. 2 c) was close to zero in vacuum (less than 9 V) even after introducing water vapors. From this point of view, the rate of hysteresis in the experiment is related to the level of water vapors present in the sensor surroundings. However, the overall graphene p-doping relates

to ambient conditions, since the average p-doping of graphene is recovered after a day of ambient atmosphere exposure. Furthermore (see below discussion), these experimental results will be explained as a consequence of different behavior of water above and under graphene with RH.

Although the presented experiments performed in vacuum conditions introduced the behavior of graphene FET sensor exposed to water molecules only, most of the recent biosensors operate in real atmospheric conditions at a presence of all other atmospheric molecules and at a standard pressure. Below, we will focus to the sensor behavior in atmosphere in more details.

Sensor response to an individual back-gate voltage step

Since a typical back-gate trace measurement consists of continual gradual changes of back-gate voltage, it is fundamental to understand the sensor response on an individual back-gate voltage step applied under atmospheric conditions at different RH. Such a measurement is shown in Fig. 3. Here, a single 70 V back-gate voltage step was applied at the time 100 s after the beginning of the transport measurement and then the resistance response was observed for the next 160 minutes. According to practice in sensing experiments[1,28–32], the relative change of resistance is depicted in Fig. 3 instead of the absolute change of resistance. The relative change of resistance is defined as: $\Delta R = (R(t) - R_0)/R_0$, where $R(t)$ is the resistance measured in time t, and R_0 is the initial resistance.

The back-gate voltage step results in a big and sudden change in relative resistance (Fig. 3 – initial part). This change approaches a value of 110 % independent of relative humidity and is caused by a compensation of the originally p-doped graphene (Fig. 2 b – blue curve) by the influx of electrons. After the application of gate-voltage, a gradual exponential decrease of relative resistance was observed with time (Fig. 3 – following part). The decay was faster for higher RH. While for 5% RH (green curve) the resistance remained almost the same (from $\Delta R = 110$ % to $\Delta R = 102$ %), for 70 % RH (brown curve) the relative resistance change dropped to 55 % (from $\Delta R = 110$ % to $\Delta R = 55$ %). Although this exponential decrease occurs within a relatively long time (160 minutes), it represents one of the main reasons for hysteresis in atmospheric back-gate trace measurements (Fig. 2 a). This is supported by the

fact, that all the time during the back-gate trace measurements (Fig. 2 a, c), the resistance also exponentially descends (Fig. 3), while the gate-voltage is continually changed.

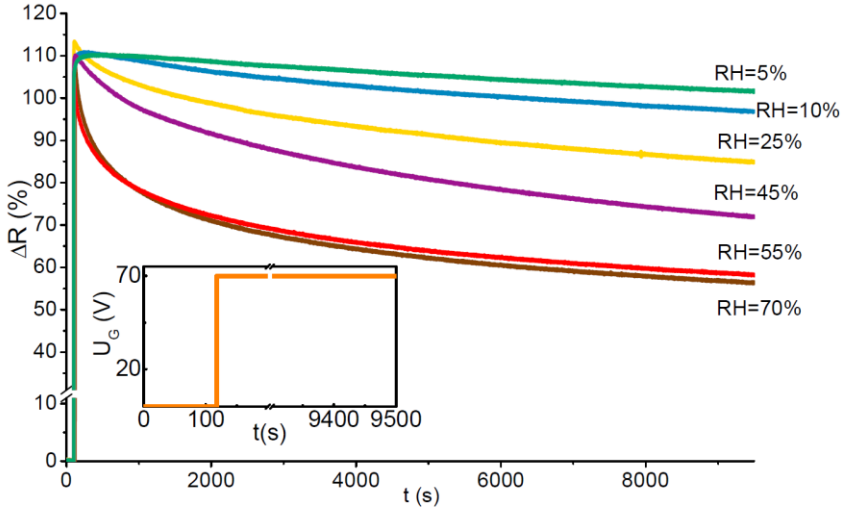

FIG. 3. Relative change of sensor resistivity caused by the application of a gate voltage step at the time 100 s from the start of experiment (see the inset) and its time evolution in the next 160 minutes under atmospheric conditions for different RH.

Sensor response to a back-gate voltage of different size in UHV and atmospheric conditions

The necessity of water vapor presence for the existence of hysteresis in the ambient atmosphere was indirectly confirmed by measurements in UHV (Fig. 4), where two gate-voltage steps of 28 V and 70 V were applied. Here, no exponential decrease after switching on the gate-voltage was observed, which corresponded to the fact that the back-gate trace experiment did not exhibit any hysteresis in UHV (Fig. 2 b).

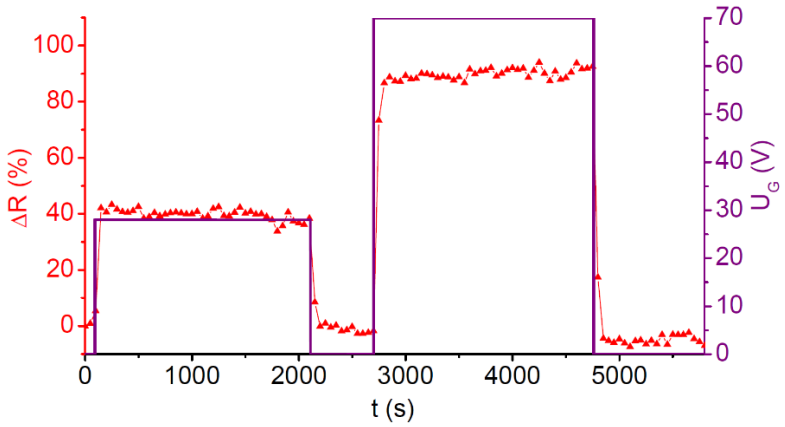

FIG. 4. Relative change of sensor resistivity after application of two gate voltage steps of 28 V (electric field intensity in SiO_2: 1 MV/cm) and 70 V (2.5 MV/cm), and its time evolution in UHV conditions before annealing.

The applied back-gate voltage 28 V and 70 V resulted in two different electric fields in the SiO_2 layer equal to 1 MV/cm and 2.5 MV/cm, respectively. Consequently, the lower 28 V gate-voltage step caused the lower resistance change $\Delta R = 40$ % than the bigger 70 V gate-voltage step which led to $\Delta R = 90$ % (Fig. 4). The exponential decay is not present in UHV (Fig. 4). If these voltages are applied in atmospheric condition, an exponential decay appears, which is for the lower gate voltage slower than for the higher one (Fig. 5). Here, the relative change of resistance related to the initial maximum R_{max} obtained after the application of the corresponding gate-voltage is defined as $\Delta R_{max} = (R(t) - R_{max})/R_{max}$.

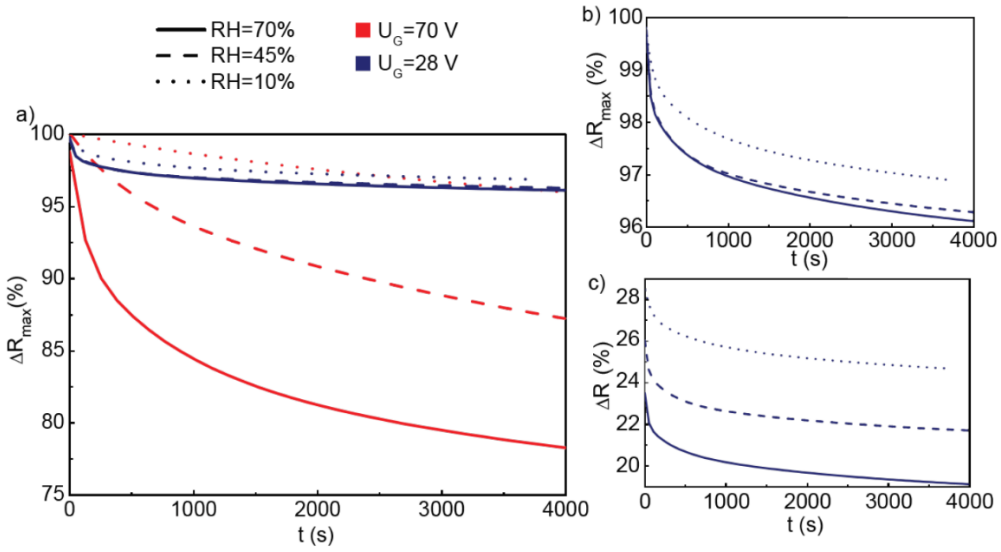

FIG. 5. (a) Relative change of sensor resistivity after application of two gate voltage steps 28 V and 70 V, and its time evolution in atmospheric conditions at relative humidities 10%, 45%, and 70%. Detail of resistivity relative change for gate voltage 28 V related to (b) an initial resistance maximum and to (c) initial resistance.

The exponential decays depicted in Fig. 3 and Fig. 5 asymptotically approach a certain saturation value of resistance response. The higher the applied gate-voltage and the relative humidity, the faster and larger the saturation process is. The hypothesis explaining this behavior will be presented in more details in Discussion.

Sensor response on an individual relative humidity step

To better understand the resistivity saturation process, the sensor resistance response to a change of relative humidity at the zero gate-voltage application was studied. As can be seen in Fig. 6, the response is relatively small (< 1.6 % relative resistance change) and had a relatively long duration (~ 50 s). Such a small response can be explained by the CNP peak-offset position of the non-annealed graphene utilized in this study which was higher than 40 V (Fig. 2 a, b - blue curve). Then, at the zero gate-voltage application ($V_G = 0$ V), the resistance can change only slightly, since the CNP peak is far away. This problem of small resistance response is usually resolved by setting a proper gate-voltage, so that the slope

of the resistance course in the back-gate voltage trace reaches its highest value – the point of maximum transconductance[33]. Nevertheless, in our case such a setting was not possible due to the mentioned process of saturation while a gate-voltage is applied for longer time. Therefore, in this article we suggest a different solution presented in the section below (part Experimental solution of hysteresis problem).

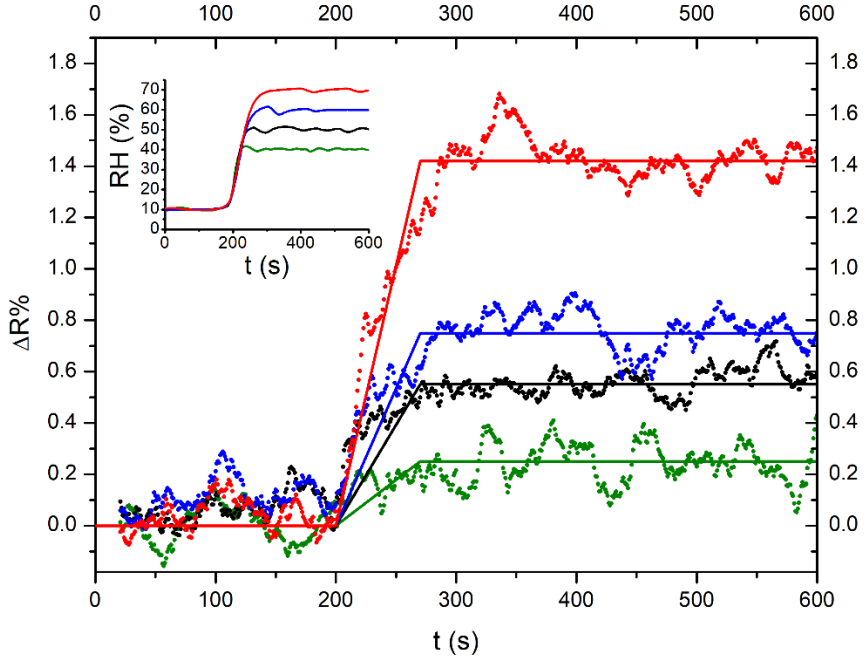

FIG. 6. Time development of the relative change of sensor resistivity after the application of 4 different step-like upturns (inset) of relative humidity at time 200 s: 10% → 40% (green), 10% → 50% (black), 10% → 60% (blue), 10% → 70% (red).

Common influence of back-gate voltage and relative humidity

In this section, the response of a graphene FET sensor to step-like relative humidity changes for different gate voltages will be discussed. Such a testing regime is often similar to a working regime of graphene sensors in real operation conditions [34–37]. In Fig. 7, the response of the graphene sensor on two relative humidity steps ($RH = 10\% \rightarrow 70\% \rightarrow 10\% \rightarrow 70\% \rightarrow 10\%$) for three different gate-voltages of -70 V, 0, and +70 V is shown. In case of the zero gate-voltage a small resistance response on humidity steps is seen, which is in agreement with our previous measurement (Fig. 6 – red curve). On the other

hand, the reaction on humidity steps is much stronger for the gate-voltages -70 and +70 V (Fig. 7 – green and red). The charts show the following behavior. First, after the application of these initial gate-voltages, the resistance change was swiftly increased and then a long exponential course followed by a saturation occurs. This typical time development was interrupted when a high relative humidity (70 %) was applied. In case of the positive gate-voltage application (+ 70 V, Fig. 7 – red curve), there is a significant initial positive increase of resistance followed by a lengthy exponential decay, which is considerably sped up during the first humidity step, meanwhile during application of the second humidity step the response is already weak and similar to the zero-gate one (black curve). In case of a negative gate-voltage application (-70 V), there is a low initial decrease of resistance followed again by an exponential time development, but at this time the growing one and accelerated in growth during the humidity step application. The response to the positive gate voltage is in agreement with the previous experiments (Fig. 3), however, the response to the negative gate voltage is quite opposite – an initial decrease followed by an exponential growth. The lower absolute initial change of resistance and its opposite character can be explained by the asymmetry of the back-gate trace curves (Fig. 2b – blue curve) since at the application of a negative voltage the resistance decreases and its absolute change is much smaller than for the positive gate voltage. Both evolutions for positive and negative gates prove the exponential tendency of returning to certain saturated values. Simultaneously, an increase of relative humidity accelerates the process of aiming towards a saturation state. This time evolution process turned on by the gate-voltage application is in competition with a small step change of resistivity caused by a change of relative humidity. During the first humidity step (Fig. 7), the domination of the returning process is evident, however, in the second step the real response on humidity prevails. The chart in Fig. 7 illustrates how the behavior of sensors can appear complex in a real experiment held in atmosphere, although it is relatively easy to explain as the interplay of the previously described three partial effects: (1) response to RH, (2) response to gate-steps and (3) motion towards saturation.

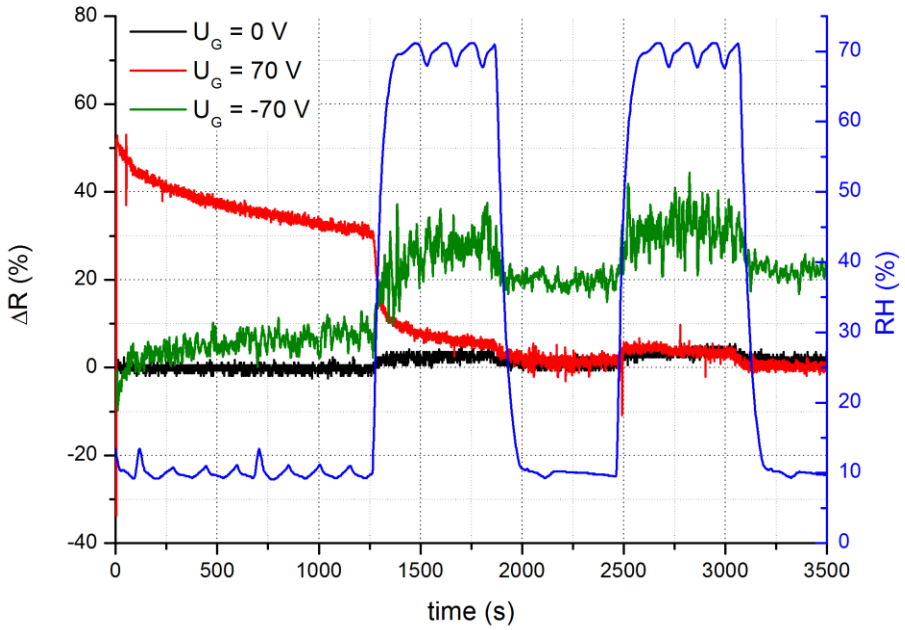

FIG. 7. Complex sensor behavior. Relative change of sensor resistivity after the application of two relative humidity steps (10% for 1250 s → 70% for 750 s → 10% for 500 s → 70% for 750 s) at three different gate-voltages 0 V, +70 V, and -70 V.

EXPERIMENTAL SOLUTION OF HYSTERESIS PROBLEM

The previous experiments has led to the following important results: The response of the sensor on an application of gate-voltage in a typical range -90 V to + 90 V is much stronger than that one on a relative humidity change ranging from 10% to 70%. Moreover, after the gate-voltage application the lengthy process of saturation occurs. However, in common continual back-gate trace measurements, an almost immediate change of resistance caused by an applied voltage is required, as the process of the long-lasting saturation (exponential course) brings a side-effect of hysteresis into the measurement. With respect to that it is reasonable to ask how to experimentally resolve the problem of hysteresis and corresponding ambiguity for sensors operating in atmosphere. This implies a specific question, what is the shortest necessary time to get a full response of a sensor on an application of gate-voltage which would not be significantly distorted by the later saturation process?

To answer this question, an experiment recording the resistance response to gate voltage pulses in small time steps was performed (Fig. 8 a, c). The resistance response to a gate voltage pulse depicted in Fig. 8b is shown in Fig. 8d. Here, the resistance was measured in 0.2 s steps after gate voltage switching. The resistance response achieved its full value approximately 2.4 s after the gate-voltage application (Fig. 8 b) and within the time interval between 2.4 s and 5 s was not affected by the exponential decay depicted in Fig. 3.

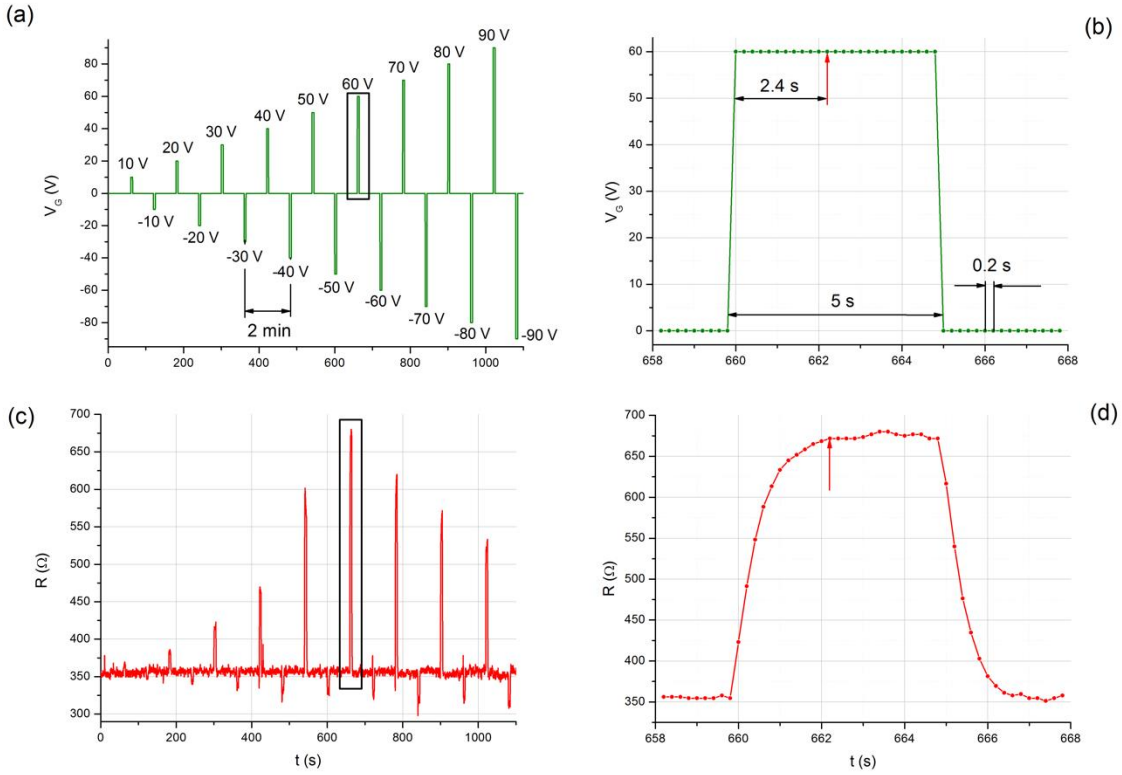

FIG. 8. The procedure of a modified back-gate trace measurement. (a) Applying a series of alternating gate-voltage pulses (each of them lasting for the short time 5 s) to eliminate the hysteresis effects caused by the exponential saturation time development, (b) the detail of a positive back gate-voltage pulse in one measurement cycle marked in (a) by the black rectangle, (c) the resistance response to the series of pulses shown in (a), and (d) detail of the resistance response marked in (c) by the black rectangle to the individual gate-voltage pulse depicted in (b).

The problem of a classical back-gate trace hysteresis lies in the long time period for which non-zero voltage is applied without an interruption, and for which the sensor tends to saturate. For example, the positive part of classical back-gate trace from 0 to 90 V and backward, almost takes 2 minutes (180 steps x 0.6 s/step = 1 min 48 s). In comparison with that, the measurement applying alternating gate-voltage eliminates the active time of measurement to 5 s.

To resolve the problem with hysteresis during sensing via back-gate voltage tracing, a series of short gate-voltage pulses and corresponding resistance responses can be utilized (Fig. 8). Such a measurement is free from hysteresis, however, it includes fewer data points than a classical continual back-gate trace measurement in the same time due to switching between time-separated discrete back-gate voltage pulses. Figure 8 (a) represents the individual measurement cycle composed from 18 gate-voltage pulses delayed from each other for 1 minute apart.

The experiment comparing a classical continual back-gate-trace measurement and the modified methodology utilizing alternating gate-voltage pulses at three different levels of relative humidity: 40%, 70%, and 10%, is done in Fig. 9.

Figures 9 a, b show the measurement performed by a standard continual back-gate voltage trace. Here, by increasing the back gate-voltage the CNP is shifted to the right (more positive gate voltages), and by decreasing the back gate-voltage it is shifted to the left. On can see this hysteresis behavior in Fig. 9 (b) as an oscillation of the maximum resistance (CNP) point in time depending on the direction of back gate-voltage changes.

The results achieved by application of alternating gate-voltage pulses are depicted in Fig. 9 c, d. Here, the sequence of gate voltages 0 V → 10 V → 0 V → -10 V → →… → 80 V → 0 V → -80 V → 0 V → 90 V → 0 V → -90 V was applied (see the inset of Fig. 9 c). The non-zero values of back-gate voltage was kept for 5 s, while the zero back-gate voltage was applied for the rest 55 s to recover the sample from previously gate-voltage application. The value of resistance was read 2.4 s after application of non-zero gate voltage. In measurements done by this way, the hysteresis behavior (difference between CNP peak

position for increasing and decreasing gate voltage) did not occur (Fig. 9 c, d), while in the continual back-gate trace the hysteresis was present (Fig. 9 a, b). At the high relative humidity 70 %, the CNP peak was 80 V (Fig. 9 c – blue curve), for the low RH = 10 % the CNP peak was 60 V (red curve), and for the middle level RH = 40 %, it was 70 V. Contrary to the standard back-gate voltage trace, there is no CNP oscillation and the sensor reacted on the level of RH only. Hence, the utilization of the alternating back-gate trace solves the problem of hysteresis by minimization of the time of gate-voltage application (avoiding the lengthy saturation process), and by application of zero gate-voltage (resuming the original equilibrium in the system).

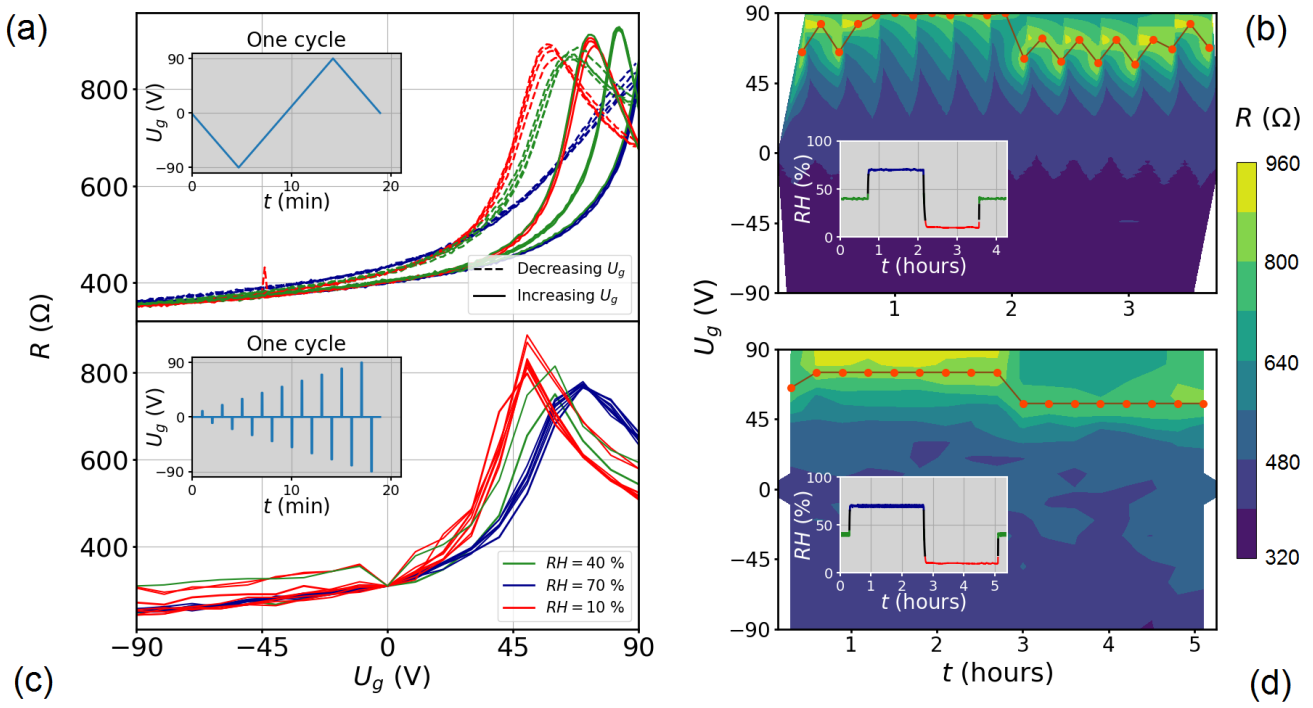

FIG. 9. Back-gate voltage trace experiment using (a, b) a standard continual procedure (see the inset in a), and (c, d) an improved method based on alternating back-gate voltage pulses (see the inset in c) at three values of relative humidities as 40%, 70%, and 10% (see the inset in b, d). The positions of maximum resistance (mostly equal to CNP) highlighted by red dots indicate a presence of hysteresis in case of the standard continual procedure (b), and the absence of hysteresis in case of the improved method (d).

DISCUSSION

In the previous chapters, the problem of hysteresis accompanying the sensor response in atmospheric conditions, its enhancement with higher humidity, and a solution by application of short alternating gate-voltage pulses instead of the continuous back-gate tracing was described. The remaining question is what is the reason behind the hysteresis appearance, and what are the fundamental causes for it?

To propose a consistent explanation, two assumptions with respect to water behavior at the graphene-water interface will be done.

First, let's assume the physisorbed water cover a graphene surface at a certain relative humidity. The presence of such a water coverage in form of droplets was directly proven by Hong et al.[38] using an environmental scanning electron microscope (ESEM). Unlike chemisorbed water (e. g. in form of OH groups) and water confined under graphene, the amount of water physisorbed on graphene is changing quite flexibly with the relative humidity.

Second, the physisorbed water can bind electrons (due to a relatively high electron affinity reaching a value of 0.8 eV for water surface[39]). Therefore, water can trap some mobile electrons from graphene, and make them immobile. Here by immobility, the removal of electrons from graphene charge carriers is meant. Since, the electrons trapped by water can still move by much slower diffusion processes inside a water.

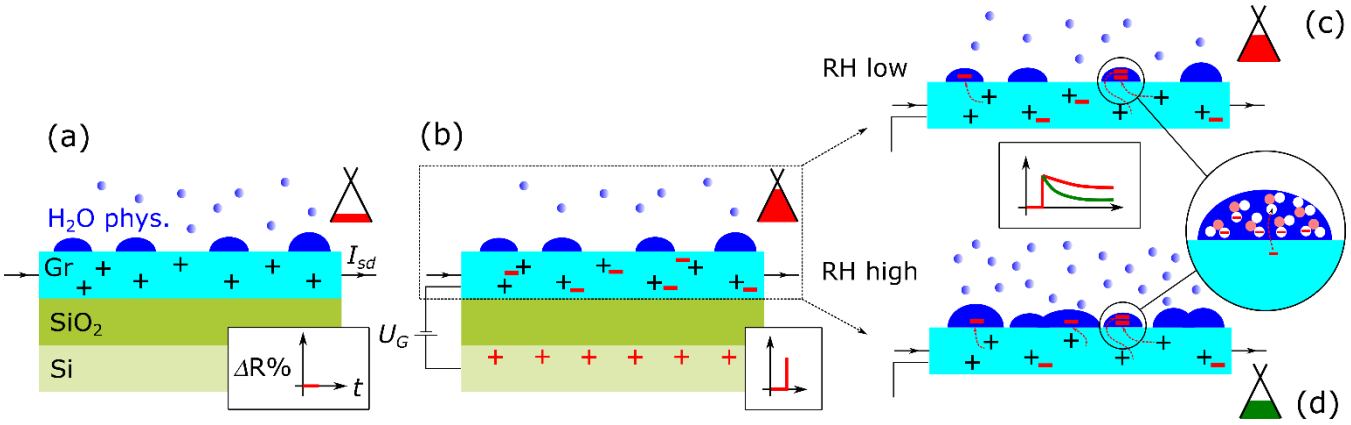

FIG. 10. Schematic of the electron trapping mechanism in physisorbed water. (a) The initial state in ambient conditions. (b) The immediate changes after the gate-voltage application. (c, d) The state after a longer gate-voltage application (c) at lower, and (d) higher humidity.

Based on this assumption, the presented experiments can be explained by the mechanism depicted in Fig. 10. Initially, proportionally to the relative humidity, water is physisorbed on the graphene surface (Fig. 10 a). As discussed above, in our experiments graphene was p doped (Fig. 2). The original graphene p-doping is probably caused by water chemisorbed to the graphene-SiO_2 interface and thus confined under graphene, and only a small fraction of this doping is caused by water physisorbed on top of the graphene. At this state, the Fermi level in graphene cone is below the Dirac point and, hence, the major charge carriers providing the source drain current (I_{sd}) are holes.

Immediately after a positive gate-voltage application, the mobile electrons flow into graphene, shifting the Fermi level up close to the Dirac point, and causing a strong resistance increase (Fig. 10 b).

After that, the electrons from graphene are being gradually trapped by water physisorbed on the graphene surface and diffuse deeper into the water droplet (Fig. 10 c). Due to this continual process, the Fermi level is shifting down further from the Dirac point, and also the resistance is decreasing. Since the trapping and diffusion of electrons in water is slow, the process having an exponential time course takes a long time (Fig. 3). At higher relative humidity, the higher amount of physisorbed water can trap more

electrons, and consequently, the process is more profound and the resistance goes down more quickly (Fig. 10 d, Fig. 3). Hence, it is worth noting that contrary to the physisorbed water molecules on the graphene surface, the concentration of chemisorbed water molecules confined under graphene is practically independent on RH[27,40] and remains the same (see below).

This phenomenon is similar to the diffusion of charge into a gate-insulating (SiO_2) layer in field effect transistors (FET)[3–13] observed when this insulating layer contains an increased number of charge traps. These traps are often produced during fabrication process of the transistor, especially by lithography steps using high energy particles (e. g. by electron beam lithography) or radiation (e. g. x-ray photons)[41–47]. If similar traps were present in our graphene-based FET sensors, then they would exhibit the hysteresis and exponential saturation also in UHV conditions, which was not true as can be seen from Fig. 2 (b), and Fig. 4. Moreover, the fabrication technology used here was much more gentle optical lithography. Hence, based on these facts, the most probable reason for the exponential decrease and saturation of the resistance with time, which is responsible for hysteresis behavior, is trapping of electrons by physisorbed water.

Generally, the graphene FET can be protected against water molecules by a suitable coverage. On the other hand, graphene in biosensors is directly exposed to water solutions, and the presented **mechanism of electron trapping by physisorbed water** can be crucial.

The relation between the source drain current I_{sd} used for resistance determination, and the applied back-gate voltage U_G can be described upon the following assumption that this current within the graphene is dependent on the absolute difference between the Fermi energy E_F and the energy of the Dirac point E_{DP}

$$I_{sd} \sim |E_F - E_{DP}| \,, \tag{1}$$

where the Fermi energy is proportional to the concentration of mobile electrons in graphene n_{Gr} as follows[39]

$$E_F = sgn(n_{Gr})\hbar v_F\sqrt{\pi|n_{Gr}|}\ . \quad (2)$$

Here, $\hbar$ is the reduced Planck constant and v_F is the Fermi velocity of electrons in graphene. The total concentration n of electrons, given by the concentration of mobile electrons in graphene n_{Gr} and concentration of immobile electrons trapped in physisorbed water on graphene n_{H_2O}, is proportional to the back-gate voltage

$$n = n_{Gr} + n_{H_2O} = \alpha \cdot V_G. \quad (3)$$

The current is determined only by electrons remaining in graphene – see Eq. (1) and (2). The resultant concentration of these electrons n_{Gr} depends on the effectivity of the trapping and diffusion of electrons inside a physisorbed water, which is lengthy process taking much more time than the fast electronic gate switching.

In the proposed model, three different processes can be distinguished according to their speed. First, the fast delivery of electrons into graphene after application of back-gate voltage taking up to 5 seconds (Fig. 8). Second, the medium-fast process of changing physisorbed water coverage after changing of relative humidity taking up to 1 minute, which was observed by Hong et al.[38] Finally, the slow process of gradual charging of physisorbed water by electrons from graphene and their diffusion into the physisorbed water taking several minutes and more (Fig. 3, Fig. 5).

In the presented explanation, the main responsibility for a hysteresis is carried out by a physisorbed water above graphene whose amount can be easily changed by relative humidity. On the other hand, the part of physisorbed water is present also under the graphene at the silica – graphene interface. However, this water is firmly captured by graphene which is for water impermeable[40]. The only way, how the water can protrude under the graphene is through the edges. This process is however extremely slow, and takes days (from 26 hrs to 70 days) even in case of a few micrometer graphene flake on silica completely submerged in water as has been proved by Lee et al.[27]. However, the onset of hysteresis, when the relative

humidity is increased, is almost immediate (Fig. 2 c). Therefore, we assume that water under the graphene is responsible for overall original p-doping (Fig. 2 c – blue curve), and after its removal by annealing in vacuum[27] the sample is almost undoped (Fig. 2 c – red curve), while the physisorbed on-graphene water easily controlled by the RH level is responsible for occurrence of hysteresis (Fig. 2 d).

CONCLUSION

The ambient transport experiments showed the hysteresis behavior of graphene sensors in a FET configuration increasing with relative humidity, and its complete elimination in UHV conditions. The origin of this hysteresis was attributed to a slow trapping of graphene electrons by water physisorbed on graphene, the amount of which is controlled by relative humidity. It is demonstrated that this problem can be resolved by application of short alternating gate-voltage pulses during back-gate trace measurement, allowing the fast electronic processes in graphene, and suppressing the slow processes as electron trapping and their diffusion in water. In FET transistors, protection cover layers of graphene can effectively eliminate the problem of hysteresis. However, in case of FET-based sensors and biosensors, where the graphene has to be exposed to ambient and water conditions, the principle and method proposed in this article should be of assistance in understanding and suppression of the hysteresis effect.

ACKNOWLEDGEMENT

We acknowledge the support by the Grant Agency of the Czech Republic (grant No. 17-21413S) and H2020 Twinning programme (project SINNCE, 810626), and MEYS CR (project No. LQ1601 – CEITEC 2020). We also acknowledge the CEITEC Nano Research Infrastructure supported by MEYS CR within the Project LM2015041 for providing us with access to their facilities, and Miroslav Kolíbal for reading the manuscript of this text.

REFERENCES

(1) Schedin, F.; Geim, a K.; Morozov, S. V; Hill, E. W.; Blake, P.; Katsnelson, M. I.; Novoselov, K. S. Detection of Individual Gas Molecules Adsorbed on Graphene. *Nature materials* **2007**, *6* (9), 652–655.

(2) Bahamonde, J. P.; Nguyen, H. N.; Fanourakis, S. K.; Rodrigues, D. F. Recent Advances in Graphene - Based Biosensor Technology with Applications in Life Sciences. *Journal of Nanobiotechnology* **2018**, 1–17.

(3) Cazalas, E.; Childres, I.; Majcher, A.; Chung, T.-F.; Chen, Y. P.; Jovanovic, I. Hysteretic Response of Chemical Vapor Deposition Graphene Field Effect Transistors on SiC Substrates. *Applied Physics Letters* **2013**, *103* (5), 053123.

(4) Gopinadhan, K.; Jun, S. Y.; Giang, T. V.; Alan, K.; Hyunsoo, Y. The Role of Charge Traps in Inducing Hysteresis : Capacitance – Voltage Measurements on Top Gated Bilayer Graphene. *Appl. Phys. Lett.* **2011**, *99* (083109), 1–3.

(5) Zhi-Min, L.; Bing-Hong, H.; Yang-Bo, Z.; Da-Peng, Y. Hysteresis Reversion in Graphene Field-Effect Transistors. *Journal of Chemical Physics* **2015**, *044703* (February 2010), 1–4.

(6) Joshi, P.; Romero, H. E.; Neal, A. T.; Toutam, V. K.; Tadigadapa, S. A. Intrinsic Doping and Gate Hysteresis in Graphene Field Effect Devices Fabricated On. *Journal of Physics Condensed Matter* **2010**, *22*, 335214.

(7) Kuhn, M.; Silversmith, D. J. Ionic Contamination and Transport of Mobile Ions in MOS Structures. *J. Electrochem. Soc.: Solid state science* **1971**, *118* (6), 966–970.

(8) Lafkioti, M.; Krauss, B.; Lohmann, T.; Zschieschang, U.; Klauk, H.; Klitzing, K.; Smet, J. H. Graphene on a Hydrophobic Substrate : Doping Reduction and Hysteresis Suppression under

Ambient Conditions. *Nano Letters* **2010**, *10*, 1149–1153.

(9) Levesque, P. L.; Sabri, S. S.; Aguirre, C. M.; Guillemette, J.; Siaj, M.; Desjardins, P.; Szkopek, T.; Martel, R. Probing Charge Transfer at Surface Using Graphene Transistors. *Nano Letters* **2011**, *11*, 132–137.

(10) Shi, Y.; Fang, W.; Zhang, K.; Zhang, W.; Li, L. Photoelectrical Response in Single-Layer Graphene Transistors. *Small* **2009**, *5* (17), 2005–2011.

(11) Wang, H.; Wu, Y.; Cong, C.; Shang, J.; Yu, T. Hysteresis of Electronic Transport in Graphene Transistors. *ACS nano* **2010**, *4* (12), 7221–7228.

(12) Xu, H.; Chen, Y.; Zhang, J.; Zhang, H. Investigating the Mechanism of Hysteresis Effect in Graphene Electrical Field Device Fabricated on SiO_2 Substrates Using Raman Spectroscopy. *Small* **2012**, *8* (18), 2833–2840.

(13) You, A.; Be, M. A. Y.; In, I. Negative Bias Temperature Instability Mechanism : The Role of Molecular Hydrogen Negative Bias Temperature Instability Mechanism : The Role of Molecular. **2006**, *153518* (April), 2004–2007.

(14) Konečný, M.; Bartošík, M.; Mach, J.; Švarc, V.; Nezval, D.; Piastek, J.; Procházka, P.; Cahlík, A.; Šikola, T. Kelvin Probe Force Microscopy and Calculation of Charge Transport in a Graphene/Silicon Dioxide System at Different Relative Humidity. *ACS Applied Materials and Interfaces* **2018**, *10* (14), 11987–11994.

(15) Li, X.; Cai, W.; An, J.; Kim, S.; Nah, J.; Yang, D.; Piner, R.; Velamakanni, a.; Jung, I.; Tutuc, E.; et al. Large Area Synthesis of High Quality and Uniform Graphene Films on Copper Foils. *Science* **2009**, *324* (5932), 1312–1314.

(16) Procházka, P.; Mach, J.; Bischoff, D.; Lišková, Z.; Dvořák, P.; Vaňatka, M.; Simonet, P.; Varlet, A.; Hemzal, D.; Petrenec, M.; et al. Ultrasmooth Metallic Foils for Growth of High Quality

Graphene by Chemical Vapor Deposition. *Nanotechnology* **2014**, *25*, 185601 1-8.

(17) Mach, J.; Procházka, P.; Bartošík, M.; Nezval, D.; Piastek, J.; Hulva, J.; Švarc, V.; Konečný, M.; Kormoš, L.; Šikola, T. Electronic Transport Properties of Graphene Doped by Gallium. *NANOTECHNOLOGY* **2017**, *28* (41).

(18) Mach, J.; Šamořil, T.; Kolíbal, M.; Zlámal, J.; Voborny, S.; Bartošík, M.; Šikola, T. Optimization of Ion-Atomic Beam Source for Deposition of GaN Ultrathin Films. *Review of Scientific Instruments* **2014**, *85* (8).

(19) Bartošík, M.; Kormoš, L.; Flajšman, L.; Kalousek, R.; Mach, J.; Lišková, Z.; Nezval, D.; Švarc, V.; Šamořil, T.; Šikola, T. Nanometer-Sized Water Bridge and Pull-off Force in AFM at Different Relative Humidities: Reproducibility Measurement and Model Based on Surface Tension Change. *Journal of Physical Chemistry B* **2017**, *121* (3), 610–619.

(20) Ohno, Y.; Maehashi, K.; Yamashiro, Y.; Matsumoto, K. Electrolyte-Gated Graphene Field-Effect Transistors for Detecting PH and Protein Adsorption. *Nano Letters* **2009**, *9* (9), 3318–3322.

(21) Mayer, D.; Krause, H.-J.; Feng, L.; Panaitov, G.; Kireev, D.; Offenhäusser, A.; Fu, W. Biosensing near the Neutrality Point of Graphene. *Science Advances* **2017**, *3* (10), e1701247.

(22) Vieira, N. C. S.; Borme, J.; Machado, G.; Cerqueira, F.; Freitas, P. P.; Zucolotto, V.; Peres, N. M. R.; Alpuim, P. Graphene Field-Effect Transistor Array with Integrated Electrolytic Gates Scaled To. *Journal of Physics: Condensed Matter* **2016**, *28*, 085302.

(23) Fu, W.; Jiang, L.; Geest, E. P. Van; Lima, L. M. C.; Schneider, G. F. Sensing at the Surface of Graphene Field-Effect Transistors. *Advanced Materials* **2017**, *29* (1603610), 1–25.

(24) Cheng, Z.; Li, Q.; Li, Z.; Zhou, Q.; Fang, Y. Suspended Graphene Sensors with Improved Signal and Reduced Noise. *Nano Letters* **2010**, *10*, 1864–1868.

(25) Ang, P. K.; Chen, W.; Thye, A.; Wee, S.; Loh, K. P. Solution-Gated Epitaxial Graphene as PH Sensor. *J. Am. Chem Soc.* **2008**, 14392–14393.

(26) Ohno, Y.; Maehashi, K.; Matsumoto, K. Label-Free Biosensors Based on Aptamer-Modified Graphene Field-Effect. *J. Am. Chem Soc.* **2010**, *132*, 18012–18013.

(27) Lee, D.; Ahn, G.; Ryu, S. Two-Dimensional Water Diffusion at a Graphene − Silica Interface. *Journal of the American Chemical Society* **2014**, *136*, 6634–6642.

(28) Hwang, S.; Lim, J.; Goo, H.; Kyun, W.; Kim, D.; Sang, I.; Hun, J.; Lee, S.; Ha, D.; Chan, S. Chemical Vapor Sensing Properties of Graphene Based on Geometrical Evaluation. *Current Applied Physics* **2012**, *12* (4), 1017–1022.

(29) Popov, V. I.; Nikolaev, D. V; Timofeev, V. B.; Smagulova, S. A.; Antonova, I. V. Graphene-Based Humidity Sensors : The Origin of Alternating Resistance Change. *Nanotechnology* **2017**, *28*, 355501.

(30) Salehi-khojin, A.; Estrada, D.; Lin, K. Y.; Bae, M.; Xiong, F.; Pop, E.; Masel, R. I. Polycrystalline Graphene Ribbons as Chemiresistors. *Advanced Materials* **2012**, *24*, 53–57.

(31) Dan, Y.; Lu, Y.; Kybert, N. J.; Luo, Z.; Johnson, A. T. C. Intrinsic Response of Graphene Vapor Sensors 2009. *Nano Letters* **2009**, *9* (4), 1472–1475.

(32) Dan, Y.; Lu, Y.; Kybert, N. J.; Luo, Z.; Johnson, A. T. C. Intrinsic Response of Graphene Vapor Sensors 2009. **2009**, 2–5.

(33) Fu, W.; Feng, L.; Panaitov, G.; Kireev, D.; Mayer, D.; Offenhäusser, A.; Krause, H. Biosensing near the Neutrality Point of Graphene. **2017**, *2*, 1–8.

(34) Choi, S.; Kim, S.; Kim, I. Ultrafast Optical Reduction of Graphene Oxide Sheets on Colorless Polyimide Fi Lm for Wearable Chemical Sensors. *NPG* **2016**, *8*, e315.

(35) Zhang, J.; Liu, X.; Neri, G.; Pinna, N. Nanostructured Materials for Room-Temperature Gas Sensors. *Advanced Materials* **2016**, *28*, 795–831.

(36) Huang, Y.; Huang, C.; Chen, Y.; Su, C.; Tsai, Y. Effect of Substrate Topography for Graphene-Based Humidity Sensors. *Japanese Journal of Applied Physics* **2019**, *58*, SDDD04-1–5.

(37) Phan, D.; Park, I.; Park, A.; Park, C.; Jeon, K. Black P / Graphene Hybrid : A Fast Response Humidity Sensor with Good Reversibility and Stability. *Scientific Reports* **2017**, No. August, 1–7.

(38) Hong, G.; Han, Y.; Schutzius, T. M.; Wang, Y.; Pan, Y.; Hu, M.; Jie, J.; Sharma, C. S.; Mu, U.; Poulikakos, D. On the Mechanism of Hydrophilicity of Graphene. *Nano Letters* **2016**, *16*, 4447–4453.

(39) Gaiduk, A. P.; Pham, T. A.; Govoni, M.; Paesani, F. Electron Affinity of Liquid Water. *Nature communications* **2018**, *9* (247), 4–9.

(40) Xu, K.; Cao, P.; Heath, J. R. Graphene Visualizes the First Water Adlayers on Mica at Ambient Conditions. *Science* **2013**, *329* (September 2010), 1188–1191.

(41) P., T. M.; Paul, V. D. *Ionizing Radiation Effects in MOS Devices and Circuits*; Wiley: New York, 1989.

(42) Aitken, J. M.; Young, D. R.; Pan, K. Electron Trapping in Electron-Beam Irradiated SiO2. *Journal of Applied Physics* **1978**, *49* (6), 3386–3391.

(43) Sethi, R. B.; Young, D. R.; Zook, J. D. Charge Trapping In Ion-Sputtered Silicon Dioxide Films On Silicon. *Journal of Electronic Material* **1990**, *19* (3), 231–234.

(44) DiMaria, D. J.; Cartier, E.; Arnold, D. Impact Ionization, Trap Creation, Degradation, and Breakdown in Silicon Dioxide Films on Silicon. *Journal of Applied Physics* **1993**, *73* (7), 3367–3384.

(45) Cho, B. J.; Chong, P. F.; Chor, E. F.; Joo, M. S.; Yeo, I. S.; Cho, B. J.; Chong, F.; Chor, E. F. Electron-Beam Irradiation-Induced Gate Oxide Degradation Electron-Beam Irradiation-Induced Gate Oxide Degradation. *Journal of Applied Physics* **2008**, *6731* (2000).

(46) Tarrach, F.; Ch'hayder, A.; Guermazi, S. Charge Trapping and Ac Conductivity in Amorphous Silicon Oxide. *Physics Procedia* **2009**, *2* (3), 941–945.

(47) Li, H.; Liu, C.; Zhang, Y.; Qi, C.; Wei, Y. Electron Radiation Effects on the Structural and Electrical Properties of MoS2 Field Effect Transistors. *Nanotechnology* **2019**, *30*, 485201.

For TOC only

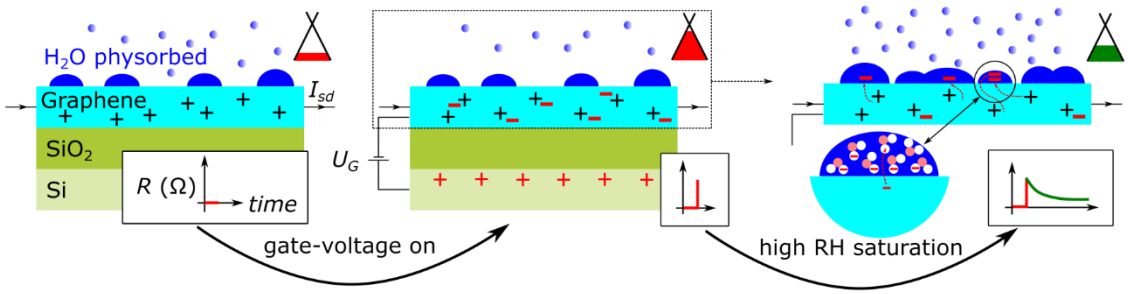
H2O physorbed
Graphene
SiO2
Si
Isd
R (Ω)
time
UG
gate-voltage on
high RH saturation